

The performance of the hot end in a plasticating 3D printer

Michael E. Mackay,^{a)} Zachary R. Swain, and Colby R. Banbury

Department of Materials Science and Engineering, University of Delaware, Newark, Delaware 19716

David D. Phan

Department of Chemical and Biomolecular Engineering, University of Delaware, Newark, Delaware 19716

David A. Edwards

Department of Mathematical Sciences, University of Delaware, Newark, Delaware 19716

(Received 19 September 2016; final revision received 21 December 2016; published 23 January 2017)

Abstract

The failure (maximum) feed velocity in a LulzBot Taz 4 3D printer at various temperatures is determined for three polymers: Acrylonitrile butadiene styrene, poly(lactic acid) (PLA), and a PLA polyhydroxybutyrate copolymer. Through an approximate solution of the energy balance, we develop a model to correlate the dimensionless fiber feed velocity (represented by a Péclet number) with a dimensionless temperature. Using these dimensionless parameters, all polymers fall onto the same curve. However, when molten polymer is forced through a small nozzle to enable 3D printing, this curve also depends on another parameter: Nozzle diameter. Our model does not account for this parameter because it does not consider hydrodynamics due to the complexity of the coupled energy and momentum balances. Thus, we modify the Péclet number to account for hydrodynamics and produce a satisfactory master curve for all diameters and polymers. Our dimensionless numbers require determining the polymer thermal and rheological properties as well as the minimum possible temperature that can be used for 3D printing of any given polymer. We discuss a way to predict this temperature based on the entry pressure drop into the nozzle. Our results will enable designers and engineers to modify the extrusion die and polymer in order to obtain better 3D printed items, and these findings can be generalized to other 3D printers. © 2017 The Society of Rheology. [<http://dx.doi.org/10.1122/1.4973852>]

I. INTRODUCTION

Until recently, the manufacture of products required machining raw materials to the desired item shape. Functionality was obtained by assembling various items to create the final product. Since the raw material, such as wood, metal, or plastic, was removed to make the item, this method was called subtractive manufacture.

Recently, a new manufacturing technology was developed that does the opposite and so is termed additive manufacture or AM [1]. In this approach, fine particles can be fused together layer-by-layer (powder bed fusion process), a monomer can be polymerized *in situ* to build up a structure (polymerization process) or thin streams of molten material can be placed on top of each other *via* extrusion through a nozzle to make the item (fused deposition modeling, FDM, or sometimes called 3D Printing). The advantage of AM is that different materials can be used simultaneously to make a heterogeneous structure on the 100 μm length scale, a fabrication that is not practical with subtractive manufacture. Currently, this technique is used to prototype a product or to

make low volume products that are not economically fabricated in any other manner.

Material extrusion has been used to make products, such as fibers and films, for decades and is performed by feeding pellets from a hopper to a plasticating screw extruder that pressurizes the melt to push it through a die. However, contemporary FDM uses a different approach: A filament of 1.5–3.0 mm diameter is fed into a heated die block with a cylindrical hole that is slightly larger than the filament, see Fig. 1, and it melts to form a seal that prohibits liquid escaping from the top. (Note FDM can also use pellet extruders so not all require a filament.)

Since the die diameter (d in Fig. 1) is very small, the pressure required to push the melt through the die is quite high. Thus, it may seem remarkable that this technique works at all, but the plasticating extruders that were used previously perform similarly: Their pressure is of order 500–1000 atm. and their pellets are successfully fed forward and melted. This success results from the forward drag flow imposed by the helical screw being larger than the backward pressure driven flow, a phenomenon that also occurs in FDM where the drag flow by feeding the fiber forward is larger than the back flow.

A recent review [2] had discussion on several models [3–5] used to calculate the pressure and temperature distribution in the die. Yet, no model has been developed to understand the heating and extrusion process so designers and

^{a)}Author to whom correspondence should be addressed; electronic mail: mem@udel.edu. Also at: Department of Chemical and Biomolecular Engineering, University of Delaware, Newark, Delaware 19716.

TABLE I. Conditions used to find the failure feed velocity in the Lulzbot Taz 4 3D printer. The temperature was decreased in 5 °C decrements.

Polymer	Nozzle diameter (mm)	Temperature range (°C)
ABS	0.35	245–175
ABS	0.50	245–165
PLA	0.35	230–150
PLA	0.50	230–145
PLAPHA	0.35	230–155
PLAPHA	0.50	230–150

feed velocity at a given setting. However, this did not pose a problem because all our tests involved manually finding the true feed velocity by measuring a length of material and the time required to feed that length into the extruder.

True feed velocity was determined by measuring 300 mm of filament and marking it with three red marks, one at the beginning of the section of filament, one at 150 mm, and one at 300 mm. This filament was fed into the printer and a timer was started as the first mark passed the top of the gear casing when viewed level to its top. Then, times were recorded when the 150 and 300 mm marks passed the same point. These two times were compared. If they were significantly different relative to the total testing time, the test was repeated until fairly consistent times were observed. If the test could not produce consistent times, the speed was taken as unstable and was lowered before testing again. Once these two times were consistent, the feed velocity was determined by dividing the 300 mm length by the total time required to feed that distance of filament.

Failure feed velocity was determined by loading each material and selecting a feed velocity that was suspected to produce total failure at the set temperature, i.e., a feed velocity so fast that the heater could not melt or soften the polymer quickly enough for successful extrusion. Once this velocity was identified such that any decrease in speed would produce successful extrusion, this feed velocity decreased by 0.1 mm/s was taken as the failure feed velocity, i.e., the fastest, but still reliable, extrusion velocity possible at the given temperature.

III. RESULTS AND DISCUSSION

A. Rheological properties

The complex viscosity was measured as a function of frequency for the polymers in this study. We used different temperatures and applied time—temperature superposition to produce the master curves shown in Fig. 2 for both the complex viscosity and the dynamic modulus. Assuming the Cox–Merz rule [6] is valid, the complex viscosity data can be fitted to a power law model, discussed in more detail below, so we can find the consistency index at the reference temperature K_{ref} and the power law index n . These parameters and the shift factors a_T are given in Table II. Finally, the modulus data show no minimum in the tangent of the phase angle suggesting the frequency was not large enough to reach the plateau modulus or there was none.

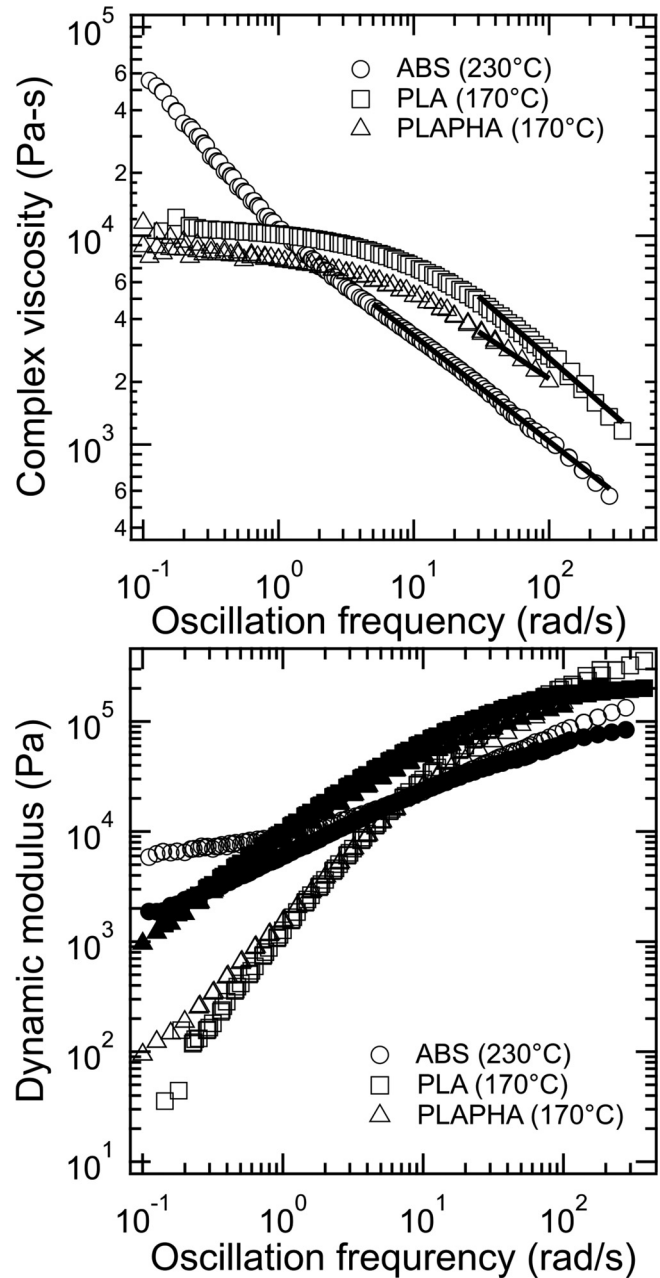


FIG. 2. Upper: Complex viscosity as a function of oscillation frequency for the three polymers considered in this study. The temperature in parentheses is the reference temperature. The solid lines are power law fits to the data assuming the Cox–Merz rule is valid. Lower: Dynamic modulus for the same materials in the upper figure, open symbols represent the storage modulus and filled symbols the loss modulus.

For PLAPHA, data below 170 °C could not be used because the results did not fall on the master curve. DSC measurements for this range (supplementary material [7]) show that there is a phase transition below this temperature and the material may be phase separating due to its copolymer structure. Since a master curve could be obtained for temperatures above 170 °C, we assume there is only one significant thermal process occurring and that is due to the temperature dependence of the relaxation time. For ABS, the terminal viscosity could not be determined because it may occur below the frequencies studied.

TABLE II. Properties of the materials used in this study.

Polymer	K_{ref} (Pa s ^{<i>n</i>})	η_T (Pa s)	a_T^a
	<i>n</i>	T_η (K)	
ABS	1.04×10^4	6.77×10^{-10}	2.79 (210)
	0.493	10 700	1.77 (220)
			1 (230)
PLA	3.54×10^4	6.27×10^{-13}	0.732 (240)
	0.433	12 400	0.525 (250)
			3.49 (150)
PLAPHA	1.50×10^4	3.37×10^{-18}	1 (170)
	0.569	17 800	0.277 (280)
			1 (170)
	C_p (kJ/kg K)	ρ (kg/m ³)	k (J/m s K)
ABS	2.1	1.15	0.21
PLA	1.7	1.25	0.13
PLAPHA	1.6	1.25	0.13

^aThe number in parentheses indicates the temperature in °C.

B. Model and the master curve

We performed experiments on the hot end and determined the failure feed velocity at a given temperature as explained above. Failure feed velocity V_f versus temperature T is plotted in Fig. 3.

Each polymer yields a different correlation, and there is no single trend other than the failure feed velocity increasing with temperature. In addition, there is a dependence on the nozzle diameter (0.35 mm versus 0.50 mm). Thus, the curve depends on both polymer type and flow condition, and presently no model accounts for this dependence.

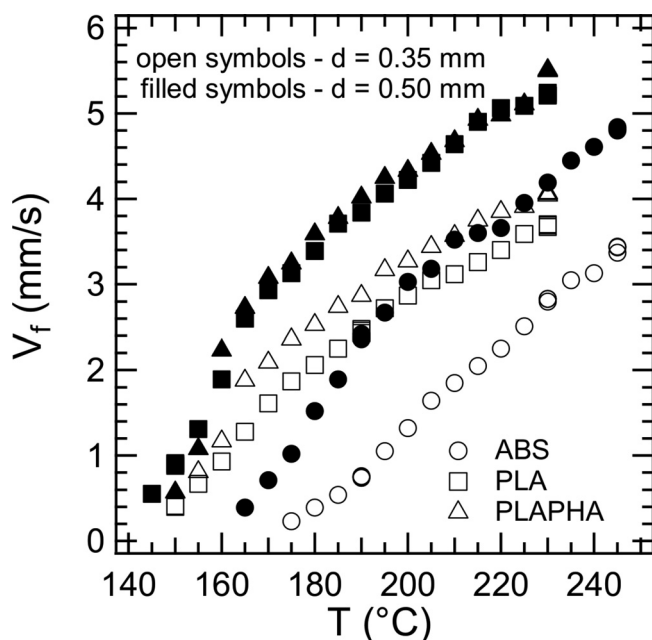


FIG. 3. Failure feed velocity (V_f) as a function of temperature that can be fed into the hot end for the polymers used here. Two different orifice diameters were used (d in Fig. 1).

Modeling the heating process for a polymer pushed into a tube is exceedingly difficult and would require a solution by numerical methods, particularly if the coupled momentum and energy balances are considered [3–5]. Instead, we consider a simplified solution using the energy balance. Our purpose is to find a parameter to represent the dimensionless failure feed velocity as a function of the dimensionless temperature of the hot end. This parameter will allow us to make a master curve of failure feed velocity that can be fed into the tube as a function of hot end temperature.

Consider a fiber of radius R_f that is fed at a velocity V_f into a heated tube with a slightly larger radius R ($\equiv D/2$) and a length H , see Fig. 1. The tube is kept at the temperature T_{hot} . The energy balance (see Bird *et al.* [8]) then simplifies to

$$\rho C_p V_f \frac{\partial T}{\partial z} = k \frac{1}{r} \frac{\partial}{\partial r} \left(r \frac{\partial T}{\partial r} \right),$$

where T is the temperature, ρ is the melt density, C_p is the melt heat capacity, k is the melt thermal conductivity, r is the radial variable, and z is the axial variable. We have assumed the steady state behavior, velocity components in the r and angular directions of zero, angular symmetry and much smaller conduction in the axial direction than the radial.

We have also assumed there is no crystallinity present in the polymer. For PLA and PLAPHA systems, the DSC traces shown in the supplementary material [7] do show a crystalline melting peak. However, there was some crystallization above the glass transition, exemplified by an exotherm that was almost equal to the melting endotherm, suggesting limited initial crystallinity. ABS is, of course, completely amorphous. We assume the melting process is much faster in the hot end and crystallization does not occur within this time frame, thus justifying our assumption of completely amorphous material for all three polymers.

The fiber is initially at temperature T_i and we solve the above equation to find the velocity so the temperature is equal to T_{min} at the centerline within the distance H . The temperature T_{min} represents the temperature where the viscosity is too large for the fiber to be fed through the tiny capillary at the end of the nozzle; it is not known at this time but its estimation will be considered below.

The full solution is given in the supplementary material [7] and it revolves around the dimensionless Péclet number Pe defined by

$$Pe = \frac{\rho C_p R^2 V_f}{k H}.$$

Although the solution given below is for small Pe , which we do not have in this experiment, we believe it is acceptable since it yields the correct temperature scaling that is not obvious.

The viscosity is assumed to follow an exponential according to

$$\eta = \eta_T \exp(T_\eta/T), \quad (1)$$

where η_T and T_η are material constants (see Table II for their values). We assume that $\eta/\eta_T \propto a_T$ to find the temperature dependence of the viscosity and so neglect any vertical shift in a stress versus shear rate curve when constructing a master curve.

We solve the energy balance by a separation-of-variables approach and compute the cross-sectional average temperature. We substitute this value into the viscosity definition, Eq. (1), and calculate the average viscosity in the tube at $z = H$. Then the solution for the conditions that have radially averaged temperature equal to T_{\min} at this axial position is given by

$$Pe = \frac{T_{\text{hot}} - T_{\min}}{T_{\min} - T_i} \frac{\beta j_{0,1}^2}{\text{Ei}\left(\frac{4\beta}{j_{0,1}^2}\right) - \ln\left(\frac{4\beta}{j_{0,1}^2}\right) - \gamma},$$

where

$$\beta \equiv \frac{T_\eta [T_{\min} - T_i]}{T_{\min}^2}$$

and $\text{Ei}(\cdot)$ is the exponential integral, $j_{0,1}$ is the Bessel function zero (2.405), and γ is Euler's constant (0.572).

In our case, the value of β is of order 10 so the solution can be approximated as

$$\begin{aligned} Pe &\approx \frac{T_\eta}{T_{\min}} \frac{T_{\text{hot}} - T_{\min}}{T_{\min}} 4\beta \exp\left(\frac{4\beta}{j_{0,1}^2}\right) \\ &\equiv T^* 4\beta \exp\left(\frac{4\beta}{j_{0,1}^2}\right), \end{aligned} \quad (2)$$

where T^* is the desired dimensionless temperature in Eq. (2). The variable β is also a dimensionless temperature and should be considered as part of the dimensionless temperature. However, since $\text{Ei}(x)$ equals $x^{-1} \exp(-x)$ for large x and T^* does include β , we believe the above definition of T^* is the best dimensionless temperature to represent the process.

A graph of Pe as a function of T^* is shown in Fig. 4. The melt thermal conductivity (k) and density (ρ) for ABS were obtained by Tadmor and Gogos [9] and those for PLA by Mortazavi *et al.* [10]. For PLAPHA, these parameters were assumed to be the same as those for PLA. The melt heat capacity (C_p) for all the polymers was determined from the DSC data in the supplementary material [7] and was an averaged value over the temperature range considered. These parameter values are given in Table II. Thus, all the variables to construct the dimensionless numbers are known *a priori* except T_{\min} . This temperature can be estimated by extrapolating the lower temperature data to zero filament velocity using the method described in Sec. III C.

If the accuracy shown in the left-hand plot of Fig. 4 were acceptable, then the correlation of $Pe = T^*$ could be used to represent the data. However, this plot shows a clear dependence on nozzle diameter, d , in Fig. 1. The model we developed does not account for nozzle diameter because it does not include hydrodynamics, neither for the flow converging into the short capillary nor for the flow in the capillary itself. So our dimensionless numbers have no d dependence at all.

According to the Hagen–Poiseuille law for flow under a given pressure drop, see Bird *et al.* [8], flow in a capillary has $V_f \propto d^2$. Thus, if hydrodynamics are not considered then V_f has no dependence on the nozzle capillary diameter, but if hydrodynamics are important then V_f has a very large diameter dependence. Since this dependence is certainly less than

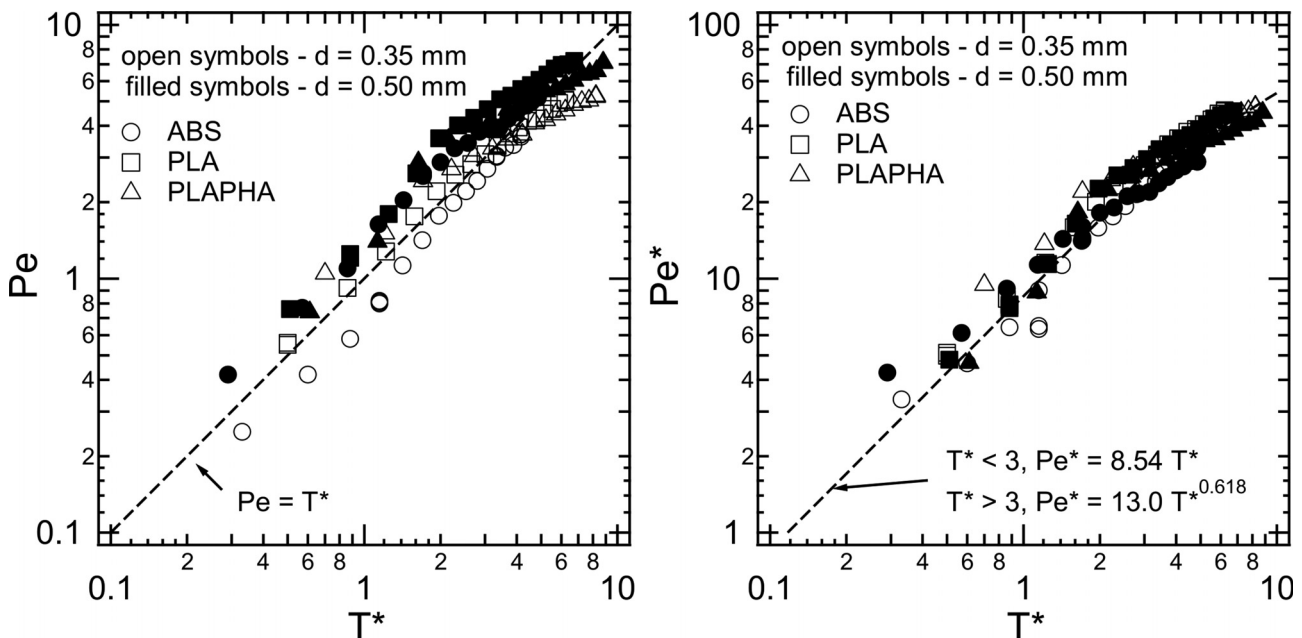


FIG. 4. Left: The Péclet number (Pe) as a function of dimensionless temperature (T^*). Both dimensionless numbers were suggested by the low Pe analysis discussed in the text. There is a systematic deviation between the large and small diameter orifice data for all polymers used. Right: Modified Péclet number (Pe^*) as a function of T^* to account for the diameter dependence.

d^2 in Fig. 4, we simply assume a linear dependence and redefine Pe to be

$$Pe^* = Pe \frac{D}{d},$$

thus using the tube diameter D to make Pe^* dimensionless.

The right-hand plot of Fig. 4 shows that this scaling of d works well and produces a single correlation. In fact, for $T^* < 3$ the correlation between Pe^* and T^* is linear (with the equation given in the figure), and above this dimensionless temperature the correlation follows a power law. The linear dependence between capillary diameter and V_f cannot be defended, but the bounds are known to be between 0 and 2 with the assumed value falling between these limits.

As stated above, all parameters are known in the definitions of Pe^* and T^* except T_{\min} . In Sec. III C, we use a hydrodynamic model to find this parameter.

C. Evaluation of T_{\min}

The temperature T_{\min} is a material parameter and is the temperature of the fiber at its centerline when it reaches the length H . At this temperature, the melt viscosity is so high that the material cannot be pushed through the capillary at the bottom of the nozzle. We will provide a method to calculate this temperature after discussing the relevant aspects of the extruder operation.

The 3D printer works by pushing the filament into the heated tube, but at a high enough feed velocity the gripping gears slip and cannot push it into the tube. This occurs at a force denoted as F_{\max} and this value is 131 ± 1 , 161 ± 2 , and 145 ± 2 N for the ABS, PLA, and PLAPHA filaments, respectively. These forces were measured by attaching a filament onto a force scale, feeding the filament into the hot end and noting the force when the filament stopped moving.

This force relates to the pressure in the tube. The tube diameter (D in Fig. 1) is 3.175 mm making the pressure in the tube approximately 20 MPa or almost 3000 psi in older units. Notably, Ramanath *et al.* [5] used finite element analysis and found the pressure in the hot end to be of order 1 MPa. Although their simulations were for a different polymer (poly- ϵ -caprolactone) and a slightly different extruder, their result agrees with ours since we are considering the limit of fiber feed velocity while they were studying much lower velocities. Regardless, the pressure in the tube is substantial and the viscosity must be exceedingly high to resist it. This pressure is denoted by P_{\max} and is equal to $F_{\max}/(\pi D^2/4)$.

Along with this pressure being high, the apparent shear rate in the orifice is also quite high. The lowest feed velocity we could measure was 0.29 mm/s and even the slower velocity of 0.05 mm/s (see below for the importance of this velocity) produces a large apparent shear rate in the die orifice. This shear rate, represented by $\dot{\gamma}_a$, is given by

$$\dot{\gamma}_a = \frac{32Q}{\pi d^3},$$

where Q is the volumetric flow rate. So for $V_f = 0.05$ mm/s, with the fiber diameter (D_f) of 2.88 mm, the apparent shear

rate is approximately 80 s^{-1} , well into the non-Newtonian regime for all the polymers (see Fig. 2).

To determine T_{\min} , we extrapolate the lowest temperature data for a given polymer to find the temperature when V_f is zero. These data will certainly fall in the non-Newtonian flow regime. Thus, flow in the converging region and into the die orifice, which is actually a very short capillary, can be modeled as a power law fluid. Then shear stress (σ) is related to the true shear rate ($\dot{\gamma}$) via a power law relation,

$$\sigma = a_T K_{\text{ref}} \dot{\gamma}^n, \quad (3)$$

where K_{ref} is the consistency index at the reference temperature. We have neglected any shift in the shear stress since this shift is much smaller than that given by the shift factor a_T . We assume the power law index (n) is temperature independent, a good assumption. Finally, we assume that $a_T \propto \exp(T_\eta/T)$, a good assumption and valid to the level of this analysis. All parameters are given in Table II.

Since we know the pressure at the fiber velocity where the gear mechanism fails for each polymer (P_{\max}), we can use this to predict V_f . We first need the pressure drop in a conical entry region followed by a short capillary. Many relations give this drop and we chose the one by Boles *et al.* [11], see also Kwon *et al.* [12]. The total pressure drop (ΔP) has components from the conical entry whose angle from the center-line to the wall is α (P_α), the entry region from the conical flow to the capillary (ΔP_o), and the flow in the capillary (ΔP_c) so

$$\Delta P = \Delta P_\alpha + \Delta P_o + \Delta P_c. \quad (4)$$

The angle α is 43.3° , see Fig. 1, so the pressure drop in the conical entry is given by

$$\begin{aligned} \Delta P_\alpha &= \frac{2a_T K_{\text{ref}}}{3n \sin(\alpha)} \left[\frac{3[3n+1]Q \sin(\alpha)}{4\pi n[1-\cos(\alpha)]^2[1+2\cos(\alpha)]} \right]^n \\ &\times \left[\frac{2^{3n}}{d^{3n}} - \frac{2^{3n}}{D^{3n}} \right] \\ &\approx a_T K_{\text{ref}} \left[\frac{3n+1}{4n} \frac{32Q}{\pi d^3} \right]^n \\ &\times \underbrace{\frac{2}{3n \sin(\alpha)} \left[\frac{3 \sin(\alpha)}{4n[1-\cos(\alpha)]^2[1+2\cos(\alpha)]} \right]^n}_{f(\alpha)}. \end{aligned} \quad (5)$$

The approximation given in the second equation comes by assuming $d \ll D$ and the term enclosed by the curly bracket is denoted as $f(\alpha)$.

The pressure drop from the conical entry into the capillary is

$$\Delta P_o = a_T K_{\text{ref}} \left[\frac{3n+1}{4n} \frac{32Q}{\pi d^3} \right]^n \frac{1.18}{n^{0.7}} \quad (6)$$

and the pressure drop from flow in the capillary is

$$\Delta P_c = a_T K_{\text{ref}} \left[\frac{3n+1}{4n} \frac{32Q}{\pi d^3} \right]^n \frac{4l}{d}, \quad (7)$$

where l is the capillary length. Given that the volumetric flow rate is $V_f \pi D_f^2 / 4$, where D_f is the fiber diameter, and that $\Delta P \equiv P_{\text{max}}$ in Eq. (4), we combine Eqs. (4)–(7) and rearrange to obtain

$$V_f = \frac{1}{2} \frac{d^3}{D_f^2} \frac{n}{3n+1} \left[\frac{P_{\text{max}}}{a_T K_{\text{ref}} \left[f(\alpha) + \frac{1.18}{n^{0.7}} + \frac{4l}{d} \right]} \right]^{1/n}. \quad (8)$$

Note T is implicit in a_T . The prediction of Eq. (8) for fiber velocity as a function of temperature is reasonably good at low temperatures and is certainly the right order of magnitude as shown in Fig. 5. It deviates most significantly from experimental data at higher temperatures that translate to higher apparent shear rates. In this region, viscoelastic effects are expected to be highest and a simple power law model to describe non-Newtonian behavior is not expected to apply [12]. Therefore, this equation is most valid at the lowest fiber velocities, precisely the regime required to determine T_{min} .

Finding T_{min} requires determining V_f with Eq. (8) for various temperatures and then extrapolating to $V_f = 0$. We find that this produces a graph of V_f versus T that is always curved, see Fig. 5, so it is impossible to accurately extrapolate. Indeed, one can keep going to lower and lower temperatures until the Newtonian flow regime is entered and an equation other than Eq. (8) is required. Even at this low fiber

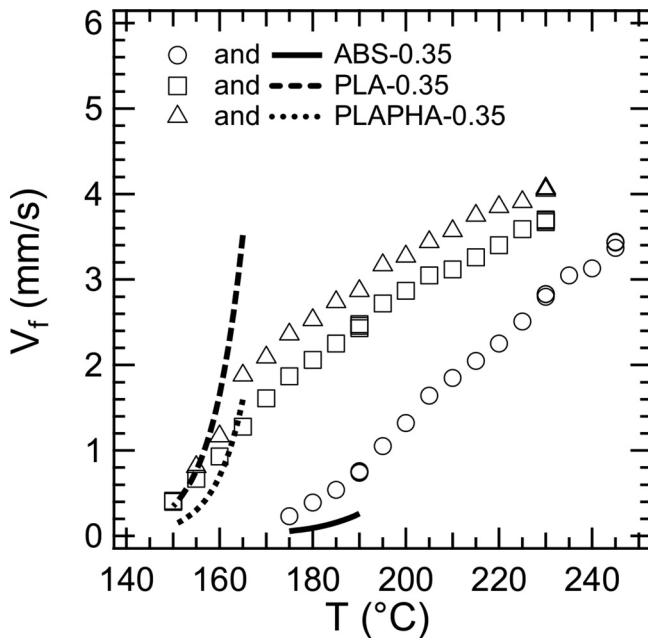


FIG. 5. Failure feed velocity as a function of temperature at a capillary diameter of 0.35 mm plotted for experimental data and for calculations with Eq. (8). The predictions span a temperature range of 15 °C which was the approximate temperature range used in the extrapolation method to determine T_{min} .

TABLE III. Comparison of experimentally determined values, via extrapolation of V_f versus T to zero fiber velocity, to the predictions of Eq. (8) at $V_f = 0.05$ mm/s for the three polymers and the two capillary diameters. Also given for each polymer is the glass transition temperature T_g .

Polymer	d	Extrapolated	Equation (8)	T_g (°C)
		T_{min} (°C)	T_{min} (°C)	
ABS	0.35	169	174	65
	0.50	160	161	
PLA	0.35	143	138	82
	0.50	138	130	
PLAPHA	0.35	148	145	86
	0.50	144	137	

feed velocity, the plot is still curved since a_T is exponentially dependent on temperature. Thus, we instead assume that T_{min} occurs when V_f is 0.05 mm/s. This is somewhat arbitrary, but we found that any assumed value near 0.05 mm/s did not change the prediction by much and that 0.05 mm/s most accurately represented the data.

The values for T_{min} are given in Table III with the average deviation being 5.5 °C with a standard deviation of 3.5 °C. We believe this is adequate to predict T_{min} for use in the correlation given in Fig. 4. For example, an error of 5 °C in T_{min} will give an error in Pe^* of approximately $\pm 20\%$ in the linear regime and $\pm 4\%$ in the power law regime, errors that are acceptable when estimating the fastest fiber velocity possible at a given temperature. Now we know *a priori* all the parameters required to find the failure feed velocity at a given temperature, allowing the use of Fig. 4.

Table III also provides the glass transition temperatures T_g determined by DSC. Comparing this parameter to T_{min} indicates that $T_{\text{min}} - T_g$ is approximately 65 °C (ABS), 82 °C (PLA), and 86 °C (PLAPHA). The mean of these differences is 78 °C so, as a crude estimation, one could use $T_{\text{min}} = T_g + 78$ °C.

Our results provide additional information. Since PLA and PLAPHA are slightly crystalline (initially less than 10%), the minimum temperature that can be used may be higher since the crystals must be melted before being heated to a certain temperature. Exactly how this melting enthalpy is incorporated into T^* is not known at present, but future studies could elucidate this effect and suggest a different definition of T_{min} or T^* . Currently, many of the polymers used in FDM are amorphous; however, efforts are being made to use different polymers and in future these will certainly include crystalline materials.

IV. CONCLUSION

We have characterized the extrusion of polymers through the hot end of a 3D printer by solving the energy balance (approximately) to develop a correlation using dimensionless variables; this master curve in Fig. 4 requires thermal and rheological characterization of the polymer. In addition, we have shown that a simple relation valid for small filament velocities

can be used to predict the minimum temperature necessary for filament extrusion. Our results will enable engineers to design the hot end and to determine the available range of fiber velocities without having to go through trial and error manufacturing processes.

It is tempting to create a model that simply balances the pressure produced by the advancing fiber to that produced by the melt entering the converging region of the nozzle [5]. In screw extrusion, this is termed balancing the extruder and die characteristics. However, in FDM the operation of the extruder is different because the fiber is being fed at a constant velocity. Furthermore, as shown in Fig. 5, predicting the pressure drop in entry flow is exceedingly difficult for higher temperatures, with the agreement between experimental and calculated data being highly unsatisfactory. As mentioned above, the model we used for entry flow is most accurate for slow flows where viscoelastic effects are minimized, which is the case at the low fiber feed velocities we used to determine T_{\min} . Since decades of research into accurately predicting the entry pressure has shown clear evidence of viscoelastic effects being important, more extensive rheological characterization is required before *a priori* prediction of the die characteristics is possible.

Here, we have considered the fastest fiber velocity possible with a 3D printer because rapid manufacture is critically needed. Faster extrusion would allow items to be fabricated much more rapidly. In addition, faster extrusion would reduce the cooling of deposited polymer between layers so adjacent layers would weld together more seamlessly. However, accomplishing successful welding requires consideration of the melt flow instabilities [13] we have observed at fiber feed velocities below the maximum. Since distorted layers due to melt fracture are undesirable, their elimination will be a subject of our future studies.

ACKNOWLEDGMENTS

The authors are grateful for funding from NIST Award No. 70NANB10H256 through the Center for Neutron Science at the University of Delaware. The authors also appreciate the partial support of this project by the Department of Materials Science and Engineering at the

University of Delaware and the help of Aleph Objects, Inc.—Makers of LulzBot 3D Printers.

References

- [1] Gibson, I., D. Rosen, and B. Stucker, *Additive Manufacturing Technologies: Rapid Prototyping to Direct Digital Manufacturing* (Springer, New York, 2010).
- [2] Turner, B. N., R. Strong, and S. A. Gold, "A review of melt extrusion additive manufacturing processes: I. Process design and modeling," *Rapid Prototyping J.* **20**, 192–204 (2014).
- [3] Yardimci, M., T. Hattori, S. Guceri, and S. Danforth, in *Solid Freeform Fabrication Proceedings*, edited by D. Bourell, J. Beaman, R. Crawford, H. Marcus, and J. Barlow (University of Texas, Austin, TX, 1997), pp. 689–698.
- [4] Bellini, A., S. Guceri, and M. Bertoldi, "Liquefier dynamics in fused deposition," *Trans. ASME J. Manuf. Sci. Eng.* **126**, 237–246 (2004).
- [5] Ramanath, H. S., C. K. Chua, K. F. Leong, and K. D. Shah, "Melt flow behaviour of poly- ϵ -caprolactone in fused deposition modelling," *J. Mater. Sci.—Mater. Med.* **19**, 2541–2550 (2008).
- [6] Cox, W. P., and E. H. Merz, "Correlation of dynamic and steady flow viscosities," *J. Polym. Sci.* **XXVIII**, 619–622 (1958).
- [7] See supplementary material at <http://dx.doi.org/10.1122/1.4973852> for the differential scanning calorimetry data for all the polymers used in this work and the derivation of Eq. (2).
- [8] Bird, R., W. Stewart, and E. Lightfoot, *Transport Phenomena*, revised 2nd ed. (Wiley, New York, 2006).
- [9] Tadmor, Z., and C. Gogos, *Principles of Polymer Processing*, 2nd ed. (John Wiley and Sons, Hoboken, NJ, 2006).
- [10] Mortazavi, B., F. Hassouna, A. Laachachi, A. Rajabpour, S. Ahzi, D. Chapron, V. Toniazzo, and D. Ruch, "Experimental and multiscale modeling of thermal conductivity and elastic properties of PLA/expanded graphite polymer nanocomposites," *Thermochim. Acta* **552**, 106–113 (2013).
- [11] Boles, R. L., H. L. Davis, and D. C. Bogue, "Entrance flows of polymeric materials: Pressure drop and flow patterns," *Polym. Eng. Sci.* **10**, 24–31 (1970).
- [12] Kwon, T. H., S. F. Shen, and K. K. Wang, "Pressure drop of polymeric melts in conical converging flow: Experiments and predictions," *Polym. Eng. Sci.* **26**, 214–224 (1986).
- [13] Agassant, J. F., D. R. Arda, C. Combeaud, A. Merten, H. Munstedt, M. R. Mackley, L. Robert, and B. Vergnes, "Polymer processing extrusion instabilities and methods for their elimination or minimisation," *Int. Polym. Process.* **21**, 239–255 (2006).